Historical eruptions of Lautaro Volcano and their impacts on lacustrine ecosystems in southern Argentina

Christoph Mayr, Rebecca E. Smith, M. Luján García, Julieta Massaferro, Andreas Lücke, Nathalie Dubois, Nora I. Maidana, Wolfgang J.-H. Meier, Holger Wissel, Bernd Zolitschka

C. Mayr, W. J.-H. Meier
Institut für Geographie, Friedrich-Alexander-Universität Erlangen-Nürnberg, Wetterkreuz 15, 91058 Erlangen, Germany
e-mail: christoph.mayr@fau.de

C. Mayr
Department für Geo- & Umweltwissenschaften and GeoBio-Center, Ludwig-Maximilians-Universität München, Richard-Wagner-Str. 10, 80333 München, Germany

R. E. Smith
Research Laboratory for Archaeology and the History of Art, 1 South Parks Road, University of Oxford, OX1 3TG, UK

M. L. García, N. I. Maidana
UBA, DBBE; CONICET-UBA, IBBEA, Laboratorio de Diatomeas Continentales, Buenos Aires, Argentina

J. Massaferro
CONICET, CENAC/APN, Bariloche, 8400, Argentina

A. Lücke, H. Wissel
Forschungszentrum Jülich GmbH, Institut für Bio- und Geowissenschaften, IBG-3: Agrosphäre, 52425 Jülich, Germany

N. Dubois
Department of Surface Waters - Research and Management, EAWAG, Überlandstrasse 133, 8600 Dübendorf, Switzerland,

B. Zolitschka
Universität Bremen, Institut für Geographie, GEOPOLAR, Celsiusstr. 2, 28359 Bremen, Germany

Key words: Patagonia, Northern Austral Volcanic Zone, ^{210}Pb dating, Diatoms, Geochemistry, Stable isotopes, Tephra

Abstract

Lacustrine sediment sequences were obtained from Lagunas Verde and Gemelas Este, two small lakes located east of the southern Patagonian Ice Field and close to the village of El Chaltén, in Argentinian Patagonia. Four tephra layers were identified in each of the short sediment sequences and characterised using individual glass-shard tephra chemistry to determine provenance. Bulk sediment geochemistry and diatom assemblages were analysed to understand the impact of the tephra deposits on the lake ecosystems. Age-depth models for the cores were established by ^{137}Cs and ^{210}Pb dating. Tephra deposits in Laguna Gemelas Este were dated to AD 1986-1998, 1943-1968, 1927-1955 and 1849-1892, and the tephra deposits in Laguna Verde were dated to AD 1940-1970, 1888-1934, 1871-1920, and 1536-1669, the latter interval determined by extrapolation. All tephras had similar geochemical composition and originated from volcanoes in the northern Austral Volcanic Zone. Tephra units were attributed to known historical eruptions and all but one, most likely, were from Lautaro Volcano (49° 01'S; 73° 33'W). The age of the youngest tephra (AD 1986-1998) from Laguna Gemelas Este points to Viedma Volcano (49° 22'S; 73° 19'W) as a possible source. Volcanic eruptions had a larger impact on Laguna Verde than on Laguna Gemelas Este, as expressed by changes in δ^{15}N values and diatom communities during tephra deposition. These shifts are explained by perturbations of the nitrogen cycle in the lake, associated with shifts in lacustrine primary production. Primary producers may have been affected by increased water turbidity caused by the ash fall, and consequently, used less nitrogen. Diatom assemblages in Laguna Verde showed marked reductions in numbers of planktonic/tychoplanktonic taxa, in favour of epiphytic/benthic diatom taxa, when tephra was deposited. This contrasts with Laguna Gemelas Este, in which epiphytic/benthic diatom species were generally more abundant and decreases in abundances of planktonic/tychoplanktonic taxa were not as strongly linked to tephra layers as in Laguna Verde. At Laguna Gemelas Este, flatter relief, greater fetch and/or drier climate may have contributed to generally less ecosystem variability, resulting in seemingly less environmental response to volcanic eruptions than in Laguna Verde.

Introduction

The subduction of the Antarctic plate (~49-53 °S) and the Scotia Microplate (~53-55 °S) beneath the South American continent induces volcanism in the Andean mountain range between 49 and 55 °S, referred to as the Austral Volcanic Zone (AVZ; Stern 2008). Volcanoes Lautaro and Fueguino represent the northernmost and southernmost volcanoes, respectively, of six known active volcanoes in the AVZ (Fig. 1A; Stern 2008). Late Glacial and Holocene eruption histories of the volcanoes in the AVZ have been reconstructed mainly using tephra layers deposited in soil outcrops, lake sediments, or peat sections (Kilian et al. 2003; Markgraf et al., 2003; Naranjo and Stern 2004; Stern 2004, 2008; Weller et al. 2015, 2017; Del Carlo et al. 2018). Explosive eruptions of the AVZ have also been documented in the last glacial, using long lake sediment records from Laguna Potrok Aike (51.97 °S 70.38 °W; Haberzettl et al. 2009; Wastegård et al. 2013).

Far less is known about recent, historical volcanic events in the AVZ. In particular, there is a considerable gap in knowledge regarding the historical volcanic frequency of centres in the northern Austral Volcanic Zone (NAVZ), which includes Volcanoes Lautaro, Viedma and Aguilera (Stern and Kilian 1996; Stern 2008; Fontjin et al. 2014). This is partly because of their location, which is difficult to reach, and generally ice-covered. Despite reports of historical eruptions (Lliboutry 1998; Martinic et al. 2008), few traces of them have been found in natural archives (Fontjin et al. 2014). The identification of tephras in natural archives could confirm historical reports and provide information about the explosivity of these eruptions, from the thickness and spatial distribution of the units. Moreover, previous geochemical fingerprints of NAVZ volcanoes (Stern and Kilian 1996; Stern 2008) are predominantly based on bulk tephra chemistry, instead of more accurate single-grain, glass-shard geochemistry, which has been rarely applied (Kastner et al. 2010). Closing this knowledge gap by studying lake sediment records and the individual glass-shard chemistry of tephras in the vicinity of these volcanoes was the first major aim of our study. Our second major aim was to establish the effect of historical volcanic deposition on these lake ecosystems by analysing paleoenvironmental variables in the sediment archives. The influence of volcanic ashfall on lake ecosystems has been debated in terms of changing pH, habitat, and nutrient availability (Lotter et al. 1995; Telford et al. 2004; Self et al. 2015). Such short-term disturbance of lacustrine systems by volcanic eruptions can be manifested in biological and geochemical sediment variables, but has rarely been documented in southernmost South America. One example, however, is the Lago Galletue (Chile) sediment record, in which a shift in diatom and chironomid assemblages and a decrease in organic matter content was ascribed to tephra from an eruption of Llaima Volcano (Cruces et al. 2006; Urrutia et al. 2007).

Our study was conducted in the NAVZ. The research area is close to the eastern margin of the Southern Patagonian Ice Field (SPI), and east of the Andean mountain ridge, with Mt. Fitz Roy (3406 m a.s.l.) being one of the most renowned mountain peaks in the region (Fig. 1B). The persistent southern hemisphere westerlies dominate the climate and provoke a strong humidity gradient on the leeward side

of the Andes where the study sites are located (Garreaud et al. 2013). This precipitation gradient is reflected in the vegetation distribution, with a dense *Nothofagus* forest in the west and Patagonian steppe to the east (Fig 1A, B). The influence of this humidity gradient on lacustrine habitats is of interest for ongoing paleolimnological studies. Additionally, the downwind position of lakes with respect to active volcanoes is beneficial for reconstructing eruption histories, as tephra is transported toward the sites. Nevertheless, the eruption history of NAVZ centres is still uncertain because of the remoteness of the area. After exploration of several regional lakes, the sediments of two small lakes, Laguna Gemelas Este (49.3849° S 72.8985° W, 880 m a.s.l.) and Laguna Verde (49.2090° S 72.9728° W, 560 m a.s.l.) were chosen for detailed investigation. Their climatic settings differ, but both contain continuous fine-grained sediment records with sufficient organic matter to facilitate investigations of tephra layers and the effects of volcanic ashfalls on Patagonian lake ecosystems.

The area surrounding the lakes belongs, in part, to Los Glaciares National Park. It was sparsely populated by indigenous people before European settlers arrived in the early 20th century (Madsen 1952). Construction of El Chaltén, the only village in the area, began in AD 1985 (Rodriguez 2009). Because of its remoteness and late settlement, reports about regional environmental trends and volcanic eruptions prior to that time are scarce. Although active volcanoes exist in the region, tephra records containing historical events are not yet established, mainly because of the inaccessibility of volcanic cones and the lack of studied sediment records (Fontjin et al. 2014). An exception to this is the 2000-year-long sediment record from Lago del Desierto (Fig. 1B), in which a tephra layer was ascribed to the AD 1959/60 eruption of Lautaro Volcano on the basis of the chronology (Kastner et al. 2010). Moreover, tephra layers of unknown age were reported from regional soils and attributed to Lautaro, Hudson and Monte Burney Volcanoes (Villegas et al. 2009). The area is also of great interest for paleoclimate and paleoenvironment reconstructions. Evidence of recent climate change is found in the accelerated shrinking of the SPI and adjacent glaciers, documented using tree-ring analysis, moraine dating, and remote sensing (Masiokas et al. 2009; Meier et al. 2018).

Our study is a first step to overcome the lack of limnogeological and volcanological data for the historical past in the NAVZ. The glass-shard chemical composition and age of tephra deposits in short sediment cores from Lagunas Verde and Gemelas Este were investigated and an attempt was made to attribute them to historical eruptions. The two lakes are comparable in size and morphometry, but located at two ends of a humidity gradient in the *Nothofagus* forest. Thus, results also provide insights into the behaviour of lake systems under different hydroclimate conditions and into the reaction of their nutrient cycles and diatom communities to short-term disturbances such as volcanic events.

Materials and methods

Sampling and scanning

Sediment cores were recovered in April 2017 with a percussion corer (Aquatic Research Instruments, USA) deployed from a rubber boat in 5.8 and 5.0 m of water in Laguna Verde and Laguna Gemelas Este, respectively. Limnological variables (pH, electric conductivity, water temperature) in lake surface waters were measured in the field with a Universal Pocket Meter (Multi 340i, WTW). The surface of the recovered sediment cores was fixed with floral foam, and core tubes were capped and transported to the lab where they were cut lengthwise. Sediment core GEM17-1 from Laguna Gemelas Este had a length of 37 cm, and sediment core VER17-1 from Laguna Verde had a length of 84 cm. The smoothed surface of one core half was photographed and scanned with an X-ray-fluorescence (XRF) core scanner (ITRAX, Cox Analytics) equipped with a Mo-tube. Elemental "concentrations" are in counts per second (cps) and were divided by coherence (coh) for standardisation (Hahn et al. 2014). Colour and lithologic variations were described before the cores were subsampled at one-cm intervals according to standard procedures (Ohlendorf et al. 2011). Volumetric samples (11.9 cm^3) were weighed before and after lyophilisation to obtain water content and dry bulk density (DBD) used for calculation of cumulative bulk dry mass. Sediment colours were determined with a Munsell soil colour chart on the fresh, non-oxidised sediment surface after core opening (Munsell Color 2000).

Bulk organic matter stable isotope geochemistry

Lyophilised samples were carefully homogenised with a spatula and sieved at 250 µm to obtain the fine sediment fraction, free of larger organic and minerogenic particles. An amount of the fine sediment fraction, sufficient to provide about 30 µg of nitrogen (typically 3-40 mg dry matter), was weighed into tin capsules for total nitrogen content (TN, in wt%) and stable isotope ($\delta^{15}N_{TN}$) determinations. Likewise, an amount of the fine sediment fraction sufficient to yield about 100 µg of organic carbon (typically 1-20 mg dry matter) was weighed in tin capsules for total organic carbon content (TOC, in wt%) and stable isotope ($\delta^{13}C_{TOC}$) analyses. These samples were decalcified by acid fumigation with 32% HCl for 16 hours in an empty desiccator (Harris et al. 2001) before folding and analysis. The packed samples were combusted at 1080 °C in an elemental analyser (EuroEA, Eurovector) with automated sample supply linked to an isotope ratio mass spectrometer (Isoprime, Micromass). Peak integration was used to determine TN and TOC concentrations and for calibration against elemental standards. The TOC/TN is presented as the molar ratio. All isotope results are reported in ‰ in standard δ notation, according to the equation

$$\delta = (R_{sample}/R_{standard} - 1) \cdot 1000 \quad (1)$$

where R is the isotope ratio ($^{13}C/^{12}C$, $^{15}N/^{14}N$) of the sample and an international standard (VPDB for carbon, AIR for nitrogen), respectively. Calibrated laboratory standards were used to ensure the quality of analyses and to relate the raw values to the isotopic reference scales. Although $\delta^{15}N_{TN}$ measurements

of Laguna Verde tephra layers were near the detection limit of the instrument, no signs of disturbance were recorded in the chromatographs and values were reproducible.

Radiometric dating

Activities of ^{137}Cs, ^{40}K, ^{210}Pb, and ^{226}Ra were determined by gamma spectrometry with a High-Purity-Germanium Well Detector. Excess ^{210}Pb data were obtained by subtracting ^{226}Ra from total ^{210}Pb activity (Appleby 2001). A constant-flux-constant-sedimentation (CFCS) model was used for ^{210}Pb age determination (Sanchez-Cabeza and Ruiz-Fernández 2012). To approach the requirements for the CFCS model, all 1-cm-thick slices containing tephra layers were removed prior to age calculations. Additionally, negative and zero ^{210}Pb activities were excluded from the age models, and one and two outliers were discarded from the base of the GEM17-1 and VER17-1 records, respectively. The ^{210}Pb activity at the sediment surface (C_0), the age and dry-mass sedimentation rates were determined from linear regression of log excess ^{210}Pb activity versus cumulative bulk dry mass, using a half-life for ^{210}Pb of 22.23 years (Sanchez-Cabeza and Ruiz-Fernández 2012). Lower and upper age estimates were determined from the sediment samples neighbouring the tephra layers, maximum and minimum errors were calculated by considering the slope error obtained in the aforementioned linear regression. Decay-corrected ^{137}Cs activities were calculated using a half-life of 30.07 years (Ribeiro Guevara and Arribére 2002).

Compositional analysis of tephra deposits

Tephra layers were identified visually, using Ca peaks from XRF scans, and with DBD anomalies. Tephra samples were wet-sieved using demineralised water and a 25-µm nylon mesh to reduce the presence of very fine-grained material, inappropriate for chemical analysis. The remaining sample was oven-dried at 50 °C and mounted in a multi-hole resin disc using SpeciFix-20 Epoxy resin (Froggatt and Gosson 1982). Once set, ground and polished, the disc was coated in carbon for chemical analysis (Lowe 2011).

The major elemental properties of individual glass shards in the sample were analysed at the Research Laboratory for Archaeology and the History of Art, University of Oxford, using a wavelength-dispersive JEOL JXA-8600 electron microprobe (EMP), equipped with four spectrometers. Where the abundance of glass shards was sufficient, thirty glass shards were analysed in each sample. All analyses were conducted with a 6-nA beam current, 15-kV accelerating voltage and a 10-µm beam diameter. To minimise element loss, sodium was analysed first. Elemental peaks were collected for 30 seconds (s), except for Na (12 s), P (60 s), Cl (50) and Mn (40 s), and for half of the total peak time on the background, either side of the peak. The machine was calibrated for each element using primary standards (minerals) prior to analysis. Also, to verify the calibration, Max Planck Institute (MPI-DING) reference glasses

were analysed at the beginning, middle and end of analytical runs (StHs6-80/G, ATHO-G, GOR132-G). Mean values for these were within 2 standard deviations of the published standard values (Jochum et al. 2006). During analysis, minerals, vesicles, and resin were avoided. To account for secondary hydration, data were normalised to 100 wt%.

Diatom analyses

An aliquot of each sample was dried at 80 °C, oxidized with H_2O_2 (30 vol%), and heated in a microwave oven for 2 minutes to eliminate organic material (Battarbee 1986). When removal of clay from the sediments was necessary, the samples were also treated following Bates et al. (1978). Samples were then rinsed repeatedly with distilled water until they reached neutral pH. Permanent slides were mounted using Naphrax®. A minimum of 400 valves per slide were counted to calculate relative abundances in percent and numbers of individuals per gram of dry sediment. Observations were made using a Reichert-Jung Polivar binocular optical microscope equipped with an immersion objective (Plan Apo 100X, NA 1.32) and differential interference contrast optics. The works of Frenguelli (1923, 1942), Metzeltin and Lange-Bertalot (1998, 2007), Rumrich et al. (2000), and Metzeltin et al. (2005) were used to identify diatom taxa.

Results

Sites and limnology

Laguna Verde is located in a humid forest with approximately 930 mm average annual precipitation (Estancia Huemules meteorological station, period 2007-2016, 1.4 km SE of the lake; Fig. 1C). The lake has an area of 0.029 km², is fed by a small inflowing creek, and is located in a basin surrounded by dense forest of *Nothofagus pumilio*. The catchment area is mountainous and has slope angles up to 40° on the western side of the lake. The lake's maximum diameter is 305 m and its maximum water depth is 5.8 m. It is surrounded by bulrush (*Schoenoplectus* sp.) and hosts few aquatic macrophytes (*Potamogeton* sp., aquatic mosses). During three visits in April (2015, 2017, 2018), electric conductivities of 20-30 µS cm^{-1}, pH values of 6.8-7.4 and temperatures of 5.2-10.2 °C were measured in the surface water.

Laguna Gemelas Este is located just above the lower tree line, which is 1 km west of the lake. The lower tree line is at an altitude of 550-650 m a.s.l. and caused by insufficient rainfall for tree growth. A meteorological station in the steppe close to the lower tree line and 5.4 km NNE from the lake receives about 305 mm average annual precipitation (Río de las Vueltas meteorological station, period 1993-2016, Fig. 1C). The name Lagunas Gemelas ("twin lakes" in Spanish) refers to two adjacent lakes, a shallow western and a deeper eastern lake. Here we report data from the eastern lake, referred to as Laguna Gemelas Este. It has no surficial inflow, an area of 0.04 km^2, a maximum diameter of 310 m, a

maximum depth of 5.2 m, and is surrounded by a patchy forest of *Nothofagus pumilio* close to the steppe-forest ecotone. A few aquatic macrophytes (aquatic mosses, *Isoetes* sp., *Myriophyllum* sp.) grow in the lake. Surface water had electric conductivities of 16-20 µS cm^{-1}, pH values of 7.2-7.7 and temperatures of 3.2-7.9 °C measured in April of the years 2015-2018.

Sedimentology and bulk-sediment geochemistry

In cores from both lakes, macroscopically visible tephra layers are characterized by high Ca content (given as Ca coh^{-1}), high DBD, and low contents of TOC and TN (Fig. 2 A, B). Tephra layers showing these characteristics occurred at 4-5, 10-15, 17-22 and below 36 cm in GEM17-1. Ca contents are missing for the latter tephra at the core base because of analytical difficulties, but a high DBD value indicates it is a tephra, as does visual identification (Fig. 2A). Similarly, tephras were detected at 5-11, 16-18, 20-28, and 54-58 cm in VER17-1. The four tephras of GEM17-1 were labelled GT1-GT4 from top to bottom, the four of VER17-1 were labelled VT1-VT4.

Sediment core GEM17-1 from Laguna Gemelas Este consists of brownish-grey (Munsell colours 2.5Y5/3, 2.5Y4/3, 2.5Y4/2), organic-rich mud intercalated with silty-to-sandy, greyish (2.5Y7/1) tephra layers (Fig. 2A). The upper part of GEM17-1 has high TOC (4-13 wt%) and TN (0.3-1.3 wt%) contents outside of tephra layers and can be classified as diatomaceous biogenic mud. The lower part (>32 cm depth) contains less TOC and TN, possibly because of a higher admixture of minerogenic components. The dark colour of a layer at 27-28 cm also appears to be of minerogenic, not organic origin, as TOC and TN do not increase. TOC/TN ratios generally vary between 6 and 24, with an exceptionally high TOC/TN ratio of 54 at 30.5 cm depth. $\delta^{13}C_{TOC}$ values range between -22 and -18‰ and $\delta^{15}N_{TN}$ between 1 and 4‰. During deposition of tephras GT1 and GT3, but not GT2, the carbon isotopic composition changes. The $\delta^{13}C_{TOC}$ values are as much as 2.6‰ lower in GT3 and 1.6‰ higher in GT1 than in sediment surrounding the tephra.

Sediment core VER17-1 from Laguna Verde consists of laminated, clayey, olive-grey mud (5Y4/2, 5Y 5/2, 5Y6/2) intercalated with four greyish to violet-greyish (5Y6/1, 7.5YR6/2), sandy tephras (Fig. 2B). Outside of the tephra layers, VER17-1 exhibited overall lower TOC (1.1-8.0 wt%) and TN contents (0.1-1.1 wt%) than GEM17-1. TOC/TN ratios range from 6 to 24. Highest TOC/TN values were reached at the base of VT3 and between VT2 and VT1. The latter peak is coincident with a TOC maximum. A second TOC maximum occurs immediately above VT4, this time coinciding with a TN maximum, increased $\delta^{13}C_{TOC}$ values and a blackish layer. $\delta^{15}N_{TN}$ values decrease by as much as 5.2‰ in each tephra layer, compared to tephra-free sections, exhibiting $\delta^{15}N_{TN}$ values between -0.5 and 2.0‰.

Radiometric dating and tephra stratigraphy

^{137}Cs data exhibit a double peak in GEM17-1 at 1.5 (82.0 Bq kg^{-1}) and 5.5 cm (69.2 Bq kg^{-1}), while ^{210}Pb activities show a distinct minimum centred at 3-5 cm sediment depth, coinciding with the low ^{137}Cs between the two peaks (Fig. 3A). The ^{137}Cs and ^{210}Pb minima are related to thin tephra layer GT1, which diluted the radioisotopes. In contrast to GEM17-1, the ^{137}Cs record of VER17-1 exhibits only a single peak with a maximum at 2-3 cm sediment depth and a steady exponential decrease of ^{210}Pb between 0 and 5 cm depth (Fig. 3B), suggesting that GT1 has no counterpart in VER17-1.

The lake sediment records were dated using excess ^{210}Pb. Tephra layers were first removed for calculation of cumulative dry mass, leading to a result of steadily increasing dry mass values with depth (Fig. 3). Exponential regressions (CFCS model) resulted in mean dry-mass sedimentation rates of 51 mg cm^{-2} a^{-1} (R^2=0.85) and 34 mg cm^{-2} a^{-1} (R^2=0.91) and extrapolated C_0 values of 168 Bq kg^{-1} and 171 Bq kg^{-1} for GEM17-1 and VER17-1, respectively.

The ^{210}Pb chronologies enable estimation of the timing of tephra deposition. For GEM17-1, the resulting age ranges were AD 1986-1998 for GT1, AD 1943-1968 for GT2, AD 1927-1955 for GT3, and AD 1849-1892 for GT4, including the error ranges (Fig. 3A). The age ranges of VER17-1 were AD 1940-1970 for VT1, AD 1888-1934 for VT2, and AD 1871-1920 for VT3 (Fig. 3B). VT4 is outside of the dated depth range because of the short half-life of ^{210}Pb. Extrapolation of the exponential regression obtained from the CFCS model, however, resulted in an estimated deposition age of AD 1536-1669.

Geochemical composition of tephra deposits

The geochemical properties of seven tephra layers (GT1, GT2, GT3, and VT1, VT2, VT3, VT4) were analysed. GT4 was not analysed because little material was available. The analysis of glass was made difficult by the high abundance of minerals. VT1 was noted as being a particularly mineral-poor sample in comparison to other analysed samples and was characterised by a greater abundance of colourless cuspate and fluted glass shards. There is no compositional difference between tephra layers (Table 1; Fig. 4). All identified tephra deposits are rhyolitic and the major elemental glass-shard chemistry suggests a similar eruptive source. Across all samples, the average silica content is 75.30 ± 1.08 wt%. The average potassium concentration is 3.37 ± 0.23 wt%, and the averaged calcium and titanium contents are 1.87 ± 0.43 wt% and 0.30 ± 0.08 wt%, respectively (Table 1).

Diatoms

For sediment core GEM17-1, diatom assemblages in all samples were analysed, except for three (16-17, 21-22 and 24-25 cm) that lacked enough material for analyses. Overall, the diatoms were well preserved, and exhibited a maximum concentration of $70 \cdot 10^6$ valves g^{-1} dry sediment at 7-8 cm depth (Fig. 5A). The total abundance was highly variable, with frequently lower concentrations if volcanic eruptions occurred. Lowest concentrations were found in the samples prior to and at the base of GT2. Only one

planktonic/tychoplanktonic taxon, *Aulacoseira* sp. 1, was found and its relative abundance fluctuates widely in the record. The taxon is most abundant in the samples between GT3 and GT4. Minimum values of *Aulacoseira* sp. 1 occur in the upper part of the core, but do not always coincide with the tephra layers. The most abundant benthic/epiphytic taxa were *Psamothidium marginulatum*, *Encyonema sileciacum*, *Nitzschia fonticola*, *Pinnularia* aff. *appendiculata*, *Sellaphora tridentula*, *Sellaphora* sp. 1, *Staurosirella* sp. 12 and *Staurosirella* sp. 8. Some benthic/epiphytic taxa, such as *Psamothidium marginulatum*, *Pinnularia* aff. *appendiculata*, and *Sellaphora tridentula* show relative abundance peaks within one or more tephra layers. *Nitzschia fonticola* reaches continuously high relative abundances after the deposition of GT3. (Fig. 5A).

The VER17-1 sediment core has an overall high diatom concentration, except when tephra layers are present. Lowest diatom abundances occurred in tephra layers VT1-VT4. The middle section of tephra VT1 (8-9 cm depth in the tephra between 5 and 11 cm) did not contain any diatoms. Diatom concentration reached its maximum value at 32 cm depth ($410 \cdot 10^6$ valves g^{-1} of dry sediment) and decreased again below. This sediment core is characterised by dominance of two *Aulacoseira* species (*Aulacoseira* sp. 1 and sp. 2), that occur in generally high relative abundances over the whole sequence, except for tephra layers, where they almost disappear, leading to short periods with dominance of benthic/epiphytic diatoms such as *Encyonema silesiacum*, *Nitzschia frustulum* var. *minutula*, small fragilarioids, *Sellaphora* sp. 1 and *Tabellaria flocculosa* (Fig. 5B).

Discussion

Regional history of explosive volcanic eruptions

Analysis of volcanic ash layers identified in the AVZ is often limited to bulk chemistry (Stern, 2008; Weller et al., 2015, 2017). This is problematic because bulk chemical analysis can be influenced by the abundance of minerals in the sample. It is therefore preferable to utilise individual-grain, glass-shard analysis to correlate between records (Fontijn et al., 2016; Del Carlo et al., 2018). There are, however, limited comparative chemical data because of the remote and often ice-covered locations of AVZ centres (and particularly NAVZ centres), and the lack of glass-shard analyses.

AVZ deposits are rich in silica, but have variable potassium as a consequence of magma variations along the volcanic arc, and as such, potassium is a useful indicator of their source (Kilian et al. 2003). For example, the widespread R_1 unit from Reclus Volcano has average SiO_2 and K_2O contents of 77.60 wt% and 2.60 wt% in its glass, respectively (Del Carlo et al. 2018). Comparatively, the widespread MB1 unit from Mt Burney Volcano has a slightly higher average SiO_2 content (78.31 wt%) and slightly lower average K_2O (2.01 wt%) in its glass (Del Carlo et al., 2018). The A_1 unit from Aguilera Volcano has average SiO_2 and K_2O contents of 75.81 wt% and 4.14 wt% in its glass, respectively (Stern, 2008). By comparison, bulk tephra and pumice analyses of the same A_1 unit yielded

much lower SiO_2 content (65.34 wt%) and K_2O content (2.26 wt%) (Stern, 2008). Analysis of glass in deposits attributed to Lautaro Volcano indicates SiO_2 and K_2O contents of ~75 wt% and ~3.3 wt%, respectively (Kastner et al., 2010), whereas bulk chemical analysis points to lower SiO_2 and K_2O contents of 65.72 wt% and 2.05 wt%, respectively (Motoki et al., 2006). The pumice in the bulk sample is reported to contain minerals such as hornblende and orthopyroxene (Motoki et al. 2006), which may have altered the analyses when compared to glass data by Kastner et al. (2010). There are no available chemical data, bulk or glass-shard, for tephra from Viedma Volcano.

The geochemical signatures of all tephra layers investigated in this study are similar, and thus indicate the same eruptive source. With respect to tephras identified from AVZ volcanoes like Monte Burney, Reclus and Aguilera (Stern 2008), the samples in GEM17-1 and VER17-1 have intermediate potassium concentrations, with an average value across all samples of 3.4 wt%. The chemical composition of volcanic deposits is in line with NAVZ deposits, as identified by Stern (2008) and Del Carlo et al. (2018). The closest volcanoes with known historical activity are Lautaro, Viedma, and possibly Aguilera (Fig. 1A, B; references in Fontjin et al. 2014). The geochemical signatures of tephra layers investigated here are congruent with those of pure glass shards from the Lago del Desierto sediment record, where a tephra was tentatively ascribed to the 1959/60 eruption of Lautaro (Kastner et al. 2010). It is, however, important to note that: i) the compositional fields of Austral Volcanic Zone volcanic centres are still relatively poorly defined, ii) there are no glass-chemistry data for Viedma Volcano, which is nearby Lautaro Volcano, iii) the high abundance of minerals in the investigated tephras resulted in a low number of chemical analyses, and iv) there is still chronological uncertainty for this historical period. As such, assignment of these layers to a historical eruptive age, based solely on the major elemental glass-shard chemistry, is not yet possible.

The chemical affinity of the deposits identified from Lagunas Gemelas Este and Verde display a similar compositional trend to that of Aguilera Volcano, but with a slightly lower potassium content (Stern 2008). As no comparable glass-shard chemistry of tephras from Lautaro, Viedma and Aguilera Volcanoes exist for comparison, assignment of these tephras in our records is based mainly on geographical and chronological evidence. We hypothesise that all but one of the tephra deposits identified in the Lagunas Gemelas Este and Verde sediment sequences originated from Lautaro Volcano, for the following reasons: 1) Lautaro Volcano is closer to the coring locations than any other AVZ volcano, except for Viedma Volcano; 2) Lautaro was the most frequently erupting NAVZ volcano in the region during the recent past (Lliboutry 1998; Motoki et al. 2006; Martinic 2008; Siebert et al. 2010; Fontijn et al. 2014) and is 42 km WNW from Laguna Verde and 60 km WNW from Laguna Gemelas Este. As winds in this area frequently blow from a northwesterly direction (Garreaud et al. 2009), tephra of Lautaro's eruptions very likely would have arrived in the area of investigation. Several confirmed eruptions have been reported from Lautaro Volcano at: AD 1978/79, 1972, 1959-60, 1945, 1933, 1883, 1878/79, and 1876 (Table 2). The only known historical eruption of Viedma Volcano was in AD 1988 (Kilian 1990; Siebert et al. 2010). Another historical eruption occurred in AD 1886. Burmeister (1891)

described widespread ash fall in the Santa Cruz Valley and other areas in Patagonia in that year, pointing to an eruption of one of the volcanoes in the NAVZ at that time. Fontjin et al. (2014) erroneously dated the eruption to AD 1891 and attributed it to Aguilera, but any other NAVZ volcano is possible. The independently dated Laguna Gemelas Este and Laguna Verde sequences indicate that the timing of the tephra units best fits the reported historical eruptions of Lautaro. This strongly suggests that Lautaro Volcano was the main source of tephra layers identified in Laguna Gemelas Este and Laguna Verde, except for GT1 (Fig. 6). The source of GT1 remains uncertain because the ^{210}Pb and ^{137}Cs chronologies disagree at this point in the sequence.

^{137}Cs is exclusively related to anthropogenic radioactive fallout from atmospheric nuclear weapons tests and nuclear accidents. Globally significant ^{137}Cs fallout started in AD 1954, reached a first maximum in AD 1959-1960, and an absolute maximum in AD 1963-1964 (Appleby 2001). In Argentina, however, maximum fallout occurred in AD 1964-1966, whereas peaks in AD 1970-1972 and AD 1974 were related to tropospheric fallout from south Pacific atmospheric nuclear weapons testing (Ribeiro Guevara and Arribére 2002). The bimodal ^{137}Cs distribution in GEM17-1 suggests that GT1 diluted the ^{137}Cs peak. Thus, the ashfall happened around or after maximum ^{137}Cs deposition, i.e. around the 1960s-1970s or later. ^{210}Pb gives a more precise date for the deposition of GT1 and relates it to the 1990s. The absence of this thin tephra layer in the ^{137}Cs record of Laguna Verde might be explained by the position of this lake outside of the fallout lobe of that specific eruption. As no major eruption was reported from Lautaro Volcano in the 1990s, the tephra most likely originated from the eruption in 1988 of Viedma Volcano, which is 28 km west of the lake (Fig. 1B). It is also possible that the ^{210}Pb dating is in error at this point in the sequence, and the ^{137}Cs may be more accurate; in that case, the deposit would likely be from the Lautaro eruption of 1978/79, because the decay-corrected ^{137}Cs nonetheless indicates a post-maximum fallout date for GT1 (Fig. 3A).

The similar ^{210}Pb age ranges of GT2 and VT1 imply that they very likely represent the same eruptive event that happened between the 1940s and 1970s. ^{210}Pb ages of VT2 and GT3 correspond less clearly in age, pointing to the same or two different eruptions in the first half of the last century. Finally, VT3 is ^{210}Pb-dated to the end of the 19th or beginning of the 20th century. Although their assignment to Lautaro Volcano is preliminary, to the best of our knowledge these tephra records represent the first evidence of frequent eruptions and widespread tephra deposition from this volcano in recently deposited lake sediments. The ^{210}Pb age ranges for tephra deposition of GT2-4 and VT1-3 fit well with historically documented eruption dates, but cannot provide accurate, annually resolved ages for the tephra layers. Among the historical eruptions reported so far, the most likely candidates for matches with our sedimentary tephra deposits, because of their elevated volcanic explosivity indices (VEI; Newhall and Self 1982), are the Lautaro eruptions of AD 1959-60 (GT2, VT1), AD 1933 (GT3, VT2), and AD 1876 or 1878/79 (GT4, VT3) (Table 2; Fig. 6). The eruptions of AD 1883 from Lautaro Volcano (Martinic 2016) or the eruption of AD 1886 (Burmeister 1891) from an unidentified volcano in the NAVZ, are also possible candidates for the tephras deposited around the end of the 19th century (Table 2; Fig. 6).

438

439 Impact of volcanic eruptions (tephra deposition) and hydroclimate on lake ecosystems

440

441 After volcanic eruptions, volcanic ash can be remobilised by wind erosion over several years in
442 Patagonia (Wilson et al. 2011). Therefore, organic matter and biogenic particles contained in the tephra
443 layers could represent not only material deposited immediately (weeks to months) after the eruption, but
444 even for several years thereafter.

445 The influence of volcanic eruptions and tephra deposition varied between the two study lakes.
446 No clear organic-geochemical changes common to all tephra layers were observed in GEM17-1. In
447 contrast, $\delta^{15}N_{TN}$ shifted to values 2.1‰ lower, on average, in the tephra layers of VER17-1, compared
448 to normal sediments (Fig. 7), whereas neither TOC/TN nor $\delta^{13}C_{TOC}$ show comparable shifts (Fig. 2).
449 Since the TOC and TN content of tephra layers is lower in VER17-1 compared to GEM17-1, any impact
450 of tephras should be more detectable in VER17-1. As the shift is evident mainly in the nitrogen isotope
451 ratios, the input of allochthonous organic matter with low $\delta^{15}N$ values during volcanic eruptions can be
452 excluded as an explanation for the $\delta^{15}N_{TN}$ shifts in VER17-1. Rather, greater inputs of allochthonous
453 organic nitrogen from terrestrial plant sources may lead to increased TOC/TN ratios (Meyers and
454 Lallier-Vergés 1999), but this is not observed for the tephra layers of VER17-1. Deposition of higher
455 amounts of soil organic matter, with comparatively low TOC/TN ratios (11-17; Mayr et al. 2009), during
456 ashfalls can also be excluded, as Patagonian soils have comparatively high $\delta^{15}N$ values (2-9‰; Mayr et
457 al. 2009). The most likely explanation therefore is a disturbance of the lacustrine nitrogen cycle
458 provoked by each eruption and lasting for the duration of the specific eruption, i.e. weeks to months.
459 Massively higher turbidity during volcanic activity, caused by ash fallout, could have led to light
460 limitation and decreased nitrogen assimilation in the lacustrine ecosystem (Finlay and Kendall 2007).
461 Lower nitrogen consumption by primary producers, such as diatoms, is associated with more negative
462 $\delta^{15}N$ values in their biomass because of less nitrate utilization (Waser et al. 1998). Because organic
463 matter content is generally very low in the tephra layers, however, low $\delta^{15}N$ values therein more likely
464 originate from inorganic nitrogen. Inorganic nitrogen concentration may have remained relatively high
465 because of reduced primary production, and became bound as ammonium in the minerogenic fraction
466 of the tephra.

467 Diatom assemblages show repeated breakdowns of planktonic/tychoplanktonic communities
468 during tephra deposition. This was more evident in Laguna Verde than in Laguna Gemelas Este (Fig.
469 5A, B). As for species composition, assemblages from Laguna Verde were completely dominated by
470 *Aulacoseira* spp. except in the tephra layers, whereas in Laguna Gemelas Este there were different
471 species with shifting relative abundances along the core. *Aulacoseira* spp. have highly silicified valves
472 and form thread-like colonies that require high water turbulence to remain suspended in the photic zone
473 of the lake (Fernandez et al. 2013; Recasens et al. 2015). A decrease of *Aulacoseira* spp. only occurs
474 during tephra deposition in VER17-1, denoting its sensitivity to volcanic ashfall. Ashfall could have

increased turbidity in the water column, increased light attenuation and reduced the depth of the photic zone. This would have diminished the development of planktonic/tychoplanktonic taxa, while non-planktonic taxa were less limited by reduced light conditions.

In Laguna Gemelas Este, epiphytic/benthic diatoms frequently dominated, and there is greater variability between planktonic/tychoplanktonic species and epiphytic/benthic ones. Diatoms have been shown to be sensitive to tephra impacts, which cause water turbidity, alter habitats, change water chemistry and nutrient availability. In response, the diatoms display changes in their abundance and/or assemblage composition (Barker et al 2000; Egan et al 2018). Lake systems, however, are variable, complex, and affected by a wide range of environmental factors (Telford et al. 2004). A clear link between changes in the diatom record and tephra deposition, as seems to be the case in Laguna Verde, is less clear in GEM17-1, and only obvious for GT2-GT4, but not for GT1 (Fig. 5A). The less clear pattern in GEM17-1 is mainly a consequence of generally higher variability between planktonic/tychoplanktonic species and epiphytic/benthic diatoms at Laguna Gemelas Este than at Laguna Verde. This higher variability can be explained by factors other than tephra deposition. First, samples with low occurrence of *Aulacoseira* sp. 1 may represent times of low lake level, as lower water level restricts their tychoplanktonic habitat and expands the areal coverage of benthic habitats. Second, Fey et al. (2009) studied Patagonian Laguna Las Vizcachas and suggested that higher amounts of epiphytic taxa could point to stronger wind-induced lateral water movements, by transporting littoral diatoms from their nearshore habitat to the lake centre. Third, less intense wind-induced turbulence could also disadvantage *Aulacoseira*, in comparison to benthic/epiphytic taxa, as the taxon is favoured by wind-induced lake turbulence (Giles et al. 2018). In summary, factors influencing diatom assemblages are more complex at Laguna Gemelas Este than at Laguna Verde, perhaps because it is situated in a more wind-exposed topographic location than is Laguna Verde.

Effects of volcanic eruptions are possibly less pronounced in the GEM17-1 record because of its more distal position in the fallout lobe, indicated by finer-grained and thinner tephra layers than those identified in VER17-1. Another possible cause for less tephra having entered Laguna Gemelas Este is the less humid climate and the flatter relief, compared to conditions at Laguna Verde. Mean angle of the slopes west of Laguna Verde is 27° and can reach values >40°, whereas Laguna Gemelas Este is located on a hillock with a slope of <2°. Thus, tephra eroded by surface runoff more easily enters Laguna Verde than Laguna Gemelas Este, even more so because the latter lacks surficial inflows, in contrast to the former.

Different hydrologic settings may have had an effect on the stable isotope values of the two sediment records as well. At the drier Laguna Gemelas Este site, $\delta^{13}C_{TOC}$ and $\delta^{15}N_{TN}$ were, on average, 5.2‰ and 1.3‰ higher, respectively, than at the more humid site, Laguna Verde (excluding tephra deposits). Surface sediments from 72 lakes along a climate gradient in western Chile showed a significant increase of $\delta^{13}C_{TOC}$ and $\delta^{15}N_{TN}$ with decreasing mean annual precipitation (Contreras et al. 2018). The causes for such humidity-dependent isotope differences could be manifold, including

different ratios of allochthonous-to-autochthonous organic matter and differences in nutrient fluxes (Mayr et al. 2009; Fan et al. 2017; Contreras et al. 2018) and cannot be disentangled without better knowledge of the carbon and nitrogen cycles in the lakes.

Conclusions

This study was a first step toward detecting and analysing tephras of historic volcanic eruptions from Lautaro Volcano, and eventually Viedma Volcano, with the ultimate goal being to better understand the impacts of volcanic ashfall on lake ecosystems in the area of El Chaltén. We found that Lautaro tephras are regionally widespread and can be used as time markers once the tephrochronologic framework is completed. We also demonstrated that the effects of ashfall can differ between lake ecosystems at similar distances from the volcano centre, probably as a consequence of different limnological conditions imposed by different climate and geomorphological settings. Ongoing studies will shed further light on the regional distribution of observed tephras and improve their tephrochronological value by studying additional lake sites and sediment variables. These data will be helpful for understanding the eruptive history of AVZ centres and provide insights into the environmental impacts of volcanic events on lacustrine ecosystems.

Acknowledgements

CM and JM acknowledge funding by BMBF (01DN16025) and cooperative project BMBF/MINCYT (AL15/03). RES was funded by NERC as part of the Environmental Research Doctoral Training Partnership at the University of Oxford (grant: NE/L002621/1). We are indebted to Ana Srur for help in the field and Sabine Stahl for assistance with XRF scanning. We thank the Los Glaciares National Park for support and permission for sampling. The provision of local meteorological data by the Argentinian Undersecretary of Water Resources of the Nation, Federico Reese, and Valeria Luvisoti, is gratefully acknowledged. We are grateful to Sebastien Bertrand and an anonymous reviewer, and to the editors, in particular Mark Brenner, for comments and suggestions on earlier versions of the manuscript.

References

Appleby PG (2001) Chronostratigraphic techniques in recent sediments. In: Last WM, Smol JP (eds) Tracking environmental change using lake sediments, Volume I: Basin analysis, coring and chronological techniques. Kluwer Academic Publishers, Dordrecht, pp 171–203

Barker P, Telford R, Merdaci O, Williamson D, Taieb M, Vincens A, Gibert E (2000) The sensitivity of a Tanzanian crater lake to catastrophic tephra input and four millennia of climate change. Holocene 10:303–310

549 Bates CD, Coxon P, Gibbard PL (1978) A new method for the preparation of clay-rich sediment samples
550 for palynological investigation. New Phytol 81:459–463
551 Battarbee RW (1986) Diatom Analysis. In: Berglund BE (ed) Handbook of Holocene Palaeoecology
552 and Palaeohydrology. J Wiley & Sons Ltd., New York, pp 527–570
553 Burmeister CV (1891) Breves datos sobre una excursión a Patagonia. Rev Museo de la Plata 2:381–394
554 Contreras S, Werne JP, Araneda A, Urrutia R, Conejero CA (2018) Organic matter geochemical
555 signatures (TOC, TN, C/N ratio, $\delta^{13}C$ and $\delta^{15}N$) of surface sediment from lakes distributed along
556 a climatological gradient on the western side of the southern Andes. Sci Total Environ 630:878–
557 888
558 Cruces F, Urrutia R, Parra O, Araneda A, Treutler H, Bertrand S, Fagel N, Torres L, Barra R, Chirinos
559 L (2006) Changes in diatom assemblages in an Andean lake in response to a recent volcanic
560 event. Arch Hydrobiol 165:23–35
561 Del Carlo P, Di Roberto A, D'Orazio M, Petrelli M, Angioletti A, Zanchetta G, Maggi V, Daga R,
562 Nazzari M, Rocchi S (2018) Late Glacial-Holocene tephra from southern Patagonia and Tierra
563 del Fuego (Argentina, Chile): A complete textural and geochemical fingerprinting for distal
564 correlations in the Southern Hemisphere. Quat Sci Rev 195:153–170
565 Egan J, Allot THE, Blackford JJ (2018) Diatom-inferred aquatic impacts of the mid-Holocene eruption
566 of Mount Mazama, Oregon, USA. Quat Res 1-16. doi:10.1017/qua.2018.73
567 Fan J, Xiao J, Wen R, Zhang S, Wang X, Cui L, Yamagata H (2017) Carbon and nitrogen signatures of
568 sedimentary organic matter from Dali Lake in Inner Mongolia: Implications for Holocene
569 hydrological and ecological variations in the East Asian summer monsoon margin. Quat Int
570 452:65–78
571 Fernández M, Björck S, Wohlfarth B, Maidana NI, Unkel I, Van der Putten N (2013) Diatom assemblage
572 changes in lacustrine sediments from Isla de los Estados, southernmost South Amerika, in
573 response to shifts in the southwesterly wind belt during last deglaciation. J Paleolimnol 50:433–
574 446
575 Fey M, Korr C, Maidana NI, Carrevedo ML, Corbella H, Dietrich S, Haberzettl T, Kuhn G, Lücke A,
576 Mayr C, Ohlendorf C, Paez MM, Quintana FA, Schäbitz F, Zolitschka B (2009)
577 Palaeoenvironmental changes during the last 1600 years inferred from the sediment record of a
578 cirque lake in southern Patagonia (Laguna Las Vizcachas, Argentina). Palaeogeogr
579 Palaeoclimatol Palaeoecol 281:363–375
580 Finlay JC, Kendall C (2007) Stable isotope tracing of temporal and spatial variability in organic matter
581 sources to freshwater ecosystems. In: Michener R, Lajtha K (eds) Stable Isotopes in Ecology
582 and Environmental Science. Blackwell, Malden, pp 283–333
583 Fontjin K, Lachowycz SM, Rawson H, Pyle DM, Mather TA, Naranjo JA, Moreno-Roa H (2014) Late
584 Quaternary tephrostratigraphy of southern Chile and Argentina. Quat Sci Rev 89:70–84

585 Frenguelli J (1923) Contribuciones para la sinopsis de las diatomeas argentinas. I Diatomeas del Río
586 Primero en la ciudad de Córdoba. Boletín de la Academia Nacional de Ciencias de Córdoba
587 27:13–119.
588 Frenguelli J (1942) Xvii Contribución al conocimiento de las diatomeas argentinas. Diatomeas del
589 Neuquén (Patagonia). Revista del Museo de La Plata (n.s.) 5 Botánica 20:73–219.
590 Froggatt PC, Gosson GJ (1982) Techniques for the preparation of tephra samples for mineral and
591 chemical analysis and radiometric dating. Department of Geology, Victoria University of
592 Wellington, 23:1–2
593 Garreaud RD, Vuille M, Compagnucci R, Marengo J (2009) Present-day South American climate.
594 Palaeogeogr Palaeoclimatol Palaeoecol 281:180–195.
595 Garreaud R, Lopez P, Minvielle M, Rojas M (2013) Large-Scale Control on the Patagonian Climate. J
596 Climate 26:215–230
597 Giles MP, Michelutti N, Grooms C, Smaol JP (2018) Long-term limnological changes in the Ecuadorian
598 páramo: Comparing the ecological responses to climate warming of shallow waterbodies versus
599 deep lakes. Freshwater Biol 63:1316–1325.
600 Global Volcanism Program (2013) Volcanoes of the World, v. 4.7.4. Venzke E (ed) Smithsonian
601 Institution. Downloaded 29 Oct 2018. https://doi.org/10.5479/si.GVP.VOTW4-2013
602 Haberzettl T, Anselmetti FS, Bowen SW, Fey M, Mayr C, Zolitschka B, Ariztegui D, Mauz B,
603 Ohlendorf C, Kastner S, Lücke A, Schäbitz F, Wille M (2009) Late Pleistocene dust deposition
604 in the Patagonian steppe - extending and refining the paleoenvironmental and
605 tephrochronological record from Laguna Potrok Aike back to 55 ka. Quat Sci Rev 28:2927–
606 2939
607 Hahn A, Kliem P, Oehlerich M, Ohlendorf C, Zolitschka B, the PASADO Science Team (2014)
608 Elemental composition of the Laguna Potrok Aike sediment sequence reveals paleoclimatic
609 changes over the past 51 ka in southern Patagonia, Argentina. J Paleolimnol 52:349–366
610 Hansen, MC, Potapov, PV, Moore R, Hancher M, Turubanova SA, Tyukavina A, Thau D, Stehman SV,
611 Goetz SJ, Loveland TR, Kommareddy A, Egorov A, Chini L, Justice CO, Townshend JRG
612 (2013) High-Resolution Global Maps of 21st-Century Forest Cover Change. Science 15:850–
613 853
614 Harris D, Horwáth WR, van Kessel C (2001) Acid fumigation of soils to remove carbonates prior to
615 total organic carbon or CARBON-13 isotopic analysis. Soil Sci Soc Am J 65:1853–1856
616 Jochum KP, Stoll B, Herwig K, Willbold M, Hofmann AW, Amini M, Aarburg S, Abouchami W,
617 Hellebrand E, Mocek B, Raczek I, Stracke A, Alard O, Bouman C, Becker S, Dücking M, Brätz
618 H, Klemd R, De Bruin D, Canil D, Cornell D, De Hoog CJ, Dalpé C, Danyushevshy L,
619 Eisenhauer A, Gao Y, Snow JE, Groschopf N, Günther D, Latkoczy C, Guillong M, Hauri EH,
620 Höfer HE, Lahaye Y, Horz K, Jacob DE, Kasemann SA, Kent AJR., Ludwig T, Zack T, Mason
621 PRD, Meixner A, Rosner M, Misawa K, Nash BP, Pfänder J, Premo WR, Sun WD, Tiepolo M,

622 Vannucci R, Vennemann T, Wayne D, Woodhead JD (2006) MPI-DING reference glasses for
623 in situ microanalysis: New reference values for element concentrations and isotope ratios.
624 Geochem Geophys Geosyst 7, Q02008, doi:10.1029/2005GC001060
625 Kastner S, Enters D, Ohlendorf C, Haberzettl T, Kuhn G, Lücke A, Mayr C, Reyss J-L, Wastegård S,
626 Zolitschka B (2010) Reconstructing 2000 years of hydrological variation derived from
627 laminated proglacial sediments of Lago del Desierto at the eastern margin of the Southern
628 Patagonian Ice Field, Argentina. Global Planet Change 72:201–214
629 Kilian R (1990) The Australandean Volcanic Zone (South Patagonia). In: Symposium international
630 "Géodynamique andine": Résumés des communication, Grenoble, France. Orstom, Paris: 301-
631 304
632 Kilian R, Hohner M, Biester H, Wallrabe-Adams HJ, Stern CR (2003) Holocene peat and lake sediment
633 tephra record from the southernmost Chilean Andes (53-55°S). Rev Geol Chile 30:23–37.
634 Lliboutry L (1998) Glaciers of the Wet Andes. In: Williams J, Ferringo R (eds) Glaciers of South
635 America. US Geological Survey Professional Paper 1386-I, pp 148–206
636 Lotter AE, Birks HJB, Zolitschka B (1995) Late-glacial pollen and diatom changes in response to two
637 different environmental perturbations: volcanic eruption and Younger Dryas cooling. J
638 Paleolimnol 14: 23–47
639 Lowe DJ (2011). Tephrochronology and its application: A review. Quat Geochronol 6:107–153.
640 Madsen A (1952) Patagonia vieja. Ciordia y Rodríguez, Buenos Aires
641 Markgraf V, Bradbury JP, Schwalb A, Burns SJ, Stern C, Ariztegui D, Anselmetti FS, Stine S, Maidana
642 N (2003) Holocene palaeoclimates of southern Patagonia: limnological and environmental
643 history of Lago Cardiel, Argentina. The Holocene 13:597–607
644 Martinic M (1988) Actividad volcánica histórica en la region de Magallanes. Rev Geol Chile 15:181–
645 186
646 Martinic M (2008) Registro historico de antecedentes volcánicos y sísmicos en la Patagonia Austral y
647 la Tierra del Fuego. Magallania 36:5–18
648 Martinic M (2016) La erupción del volcán de los gigantes (Lautaro) en 1883. Algunas Consideraciones.
649 Magallania 44:65–68
650 Masiokas M, Rivera A, Espizua LE, Villalba R, Delgado S, Aravena JC (2009) Glacier fluctuations in
651 extratropical South America during the past 1000 years. Palaeogeogr Palaeoclimatol Palaeoecol
652 281:242–268
653 Mayr C, Lücke A, Maidana NI, Wille M, Haberzettl T, Corbella H, Ohlendorf C, Schäbitz F, Fey M,
654 Janssen S, Zolitschka B (2009) Isotopic fingerprints on lacustrine organic matter from Laguna
655 Potrok Aike (southern Patagonia, Argentina) reflect environmental changes during the last
656 16,000 years. J Paleolimnol 42:81–102

Meier WJ-H, Grießinger J, Hochreuther P, Braun MH (2018) An updated multi-temporal glacier inventory for the Patagonian Andes with changes between the Little Ice Age and 2016. Front Earth Sci 6, doi: 10.3389/feart.2018.00062

Messager ML, Lehner B, Grill G, Nedeva I, Schmitt O (2016) Estimating the volume and age of water stored in global lakes using a geo-statistical approach. Nat Commun 7, 13603, doi: 10.1038/ncomms13603

Meyers P, Lallier-Vergés E (1999) Lacustrine sedimentary organic matter records of late Quaternary paleoclimates. J Paleolimnol 21:345–372

Metzeltin D, Lange–Bertalot H (1998) Tropical diatoms of South America I. About 700 predominantly rarely known or new taxa representative of the neotropical flora. Iconogr Diatomol 5:1–695

Metzeltin D, Lange–Bertalot H (2007) Tropical diatoms of South America II. Special remarks on biogeographic disjunction. Iconogr Diatomol 18:1–877

Metzeltin D, Lange–Bertalot H, García-Rodríguez F (2005) Diatoms of Uruguay. Compared with other taxa from South America and elsewhere. Iconogr Diatomol 15:1–736

Motoki A, Orihashi Y, Naranjo J, Hirata D, Skvarca P, Anma R (2006) Geologic reconnaissance of Lautaro Volcano, Chilean Patagonia. Rev Geol Chile 33:177–187

Munsell Color (2000) Munsell Soil Color Charts. Grand Rapids, USA

Naranjo JA, Stern CR (2004) Holocene tephrochronology of the southernmost part (42°30'-45°S) of the Andean Southern Volcanic Zone. Rev Geol Chile 31:224–240

Ohlendorf C, Gebhardt C, Hahn A, Kliem P, Zolitschka B, the PASADO science team (2011) The PASADO core processing strategy – A proposed new protocol for sediment core treatment in multidisciplinary lake drilling projects. Sediment Geol 239:104–115

Recasens C, Ariztegui D, Maidana NI, Zolitschka B, The PASADO Science Team (2015) Diatoms as indicators of hydrological and climatic changes in Laguna Potrok Aike (Patagonia) since the Late Pleistocene. Palaeogeogr Palaeoclimatol Palaeoecol 417:309–319

Ribeiro Guevara S, Arribére M (2002) ^{137}Cs dating of lake cores form the Nahuel Huapi National Park, Patagonia, Argentina: Historical records and profile measurements. J Radioanal Nucl Ch 252:37–45

Rodriguez DR (2009) Allá lejos El Chaltén. Honorable Cámara de Diputados de la Provincia de Santa Cruz, Rio Gallegos

Rumrich U, Lange–Bertalot H, Rumrich M (2000) Diatoms of the Andes. From Venezuela to Patagonia/Tierra del Fuego. Iconogr Diatomol 9:1–649

Sanchez-Cabeza JA, Ruiz-Fernández AC (2012) ^{210}Pb sediment radiochronology: An integrated formulation and classification of dating models. Geochim Cosmochim Acta 82:183–200

Self AE, Klimaschewski A, Solovieva N, Jones VJ, Andrén E, Andreev AA, Hammarlund D, Brooks SJ (2015) The relative influences of climate and volcanic activity on Holocene lake

development inferred from a mountain lake in central Kamchatka. Global Planet Change 134:67–81

Siebert L, Simkin T, Kimberly P (2010) Volcanoes of the world. Smithsonian Institution, Berkeley/Los Angeles

Stern C (1990) Tephrochronology of Southernmost Patagonia. Natl Geogr Res 6:110–126

Stern CR (2004) Active Andean volcanism: its geologic and tectonic setting. Rev Geol Chile 31:1–51

Stern C (2008) Holocene tephrochronology record of large explosive eruptions in the southernmost Patagonian Andes. Bull Volcanol 70:435–454

Stern CR, Kilian R (1996) Role of the subducted slab, mantle wedge and continental crust in the generation of adakites from the Andean Austral Volcanic Zone. Contrib Mineral Petrol 123:263–281

Telford RJ, Barker, P, Metcalfe S, Newton A. (2004) Lacustrine responses to tephra deposition: examples from Mexico. Quat Sci Rev 23:2337–2353

Urrutia R, Araneda A, Cruces F, Torres L, Chirinos L, Treutler HC, Fagel N, Bertrand S, Alvial I, Barra R, Chapron E (2007) Changes in diatom, pollen, and chironomid assemblages in response to a recent volcanic event in Lake Galletue (Chilean Andes). Limnologica 37:49–62

Villegas DC, Pereyra FX, Viaggio M, Ferrer JA (2009) Occurencia de materiales piroclásticos en suelos de tres sectores del oeste de Santa Cruz. Revista de la Asociación Geológica Argentina 64:303–311

Waser NAD, Harrison PJ, Nielsen B, Calvert SE, Turpin DH (1998) Nitrogen isotope fractionation during the uptake and assimilation of nitrate, nitrite, ammonium, and urea by a marine diatom. Limnol Oceanogr 43:215–224

Wastegård S, Veres D, Kliem P, Hahn A, Ohlendorf C, Zolitschka B, The PASADO Science Team (2013) Towards a late Quaternary tephrochronological framework for the southernmost part of South America – the Laguna Potrok Aike tephra record. Quat Sci Rev 71:81–90

Weller DJ, Miranda CG, Moreno PI, Villa-Martínez R, Stern CR (2015). Tephrochronology of the southernmost Andean Southern Volcanic Zone, Chile. Bull Volcanol 77:1–24

Weller DJ, de Porras ME, Maldonado A (2017). Holocene tephrochronology of the lower Río Cisnes valley, southern Chile. Andean Geol 44:229–248

Wilson TM, Cole JW, Stewart C, Cronin SJ, Johnston DM (2011) Ash storms: impacts of wind-remobilised volcanic ash on rural communities and agriculture following the 1991 Hudson eruption, southern Patagonia, Chile. Bull Volcanol 73:223–239

Figures

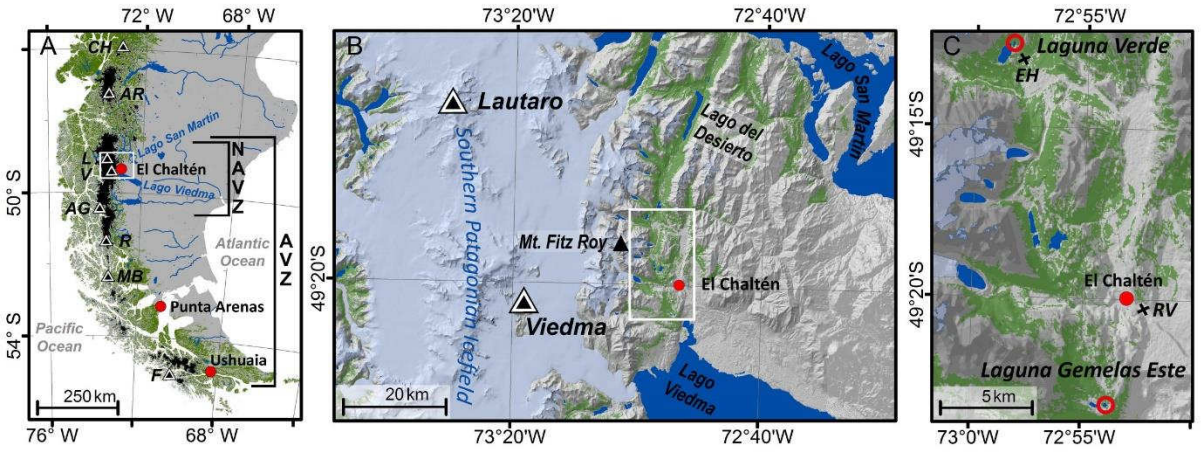

Fig. 1 (A) Map of southern South America showing the research area (box) and major active volcanoes: Cerro Hudson (CH), Arenales (AR), Lautaro (L), Viedma (V), Aguilera (AG), Reclús (R), Monte Burney (MB), Fueguino (F). The extension of the Austral Volcanic zone (AFZ) and northern Austral Volcanic Zone (NAVZ) is indicated. (B) Southern Patagonian Ice Field, subglacial Lautaro and Viedma Volcanoes, and the research area next to El Chaltén. The forested area is in green. (C) Locations of Lagunas Verde and Gemelas Este in the area around El Chaltén. Crosses mark the meteorological stations at Estancia Huemules (EH) and Río de las Vueltas (RV). Base map: SRTM, LP DACC NASA Version 3, forested area: Hansen et al. (2013), water bodies: Messager et al. (2016), glaciated area: Meier et al. (2018)

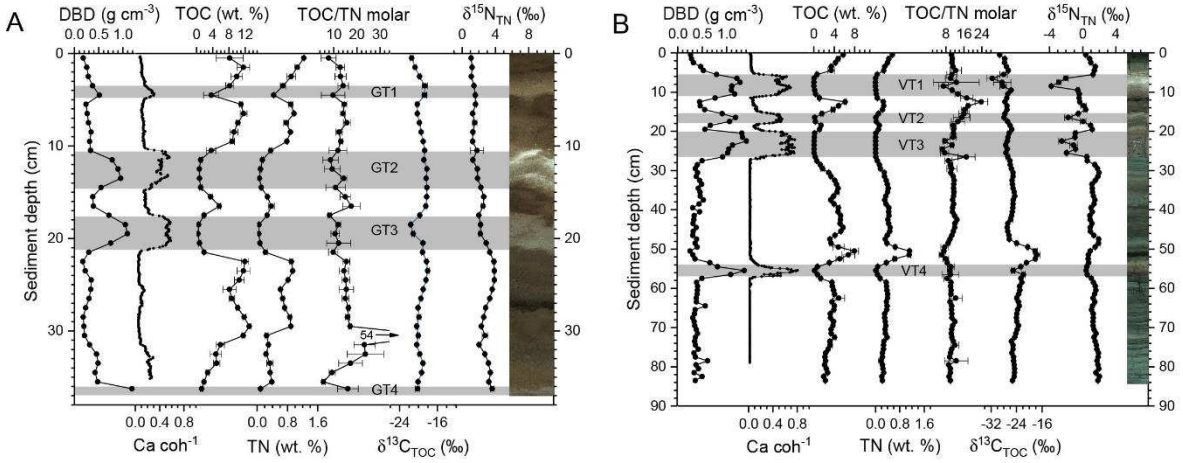

Fig. 2 Geochemical and stable isotope records and core photographs of GEM17-1 (A) and VER17-1 (B). Grey bars highlight tephra layers readily recognizable by their Ca/coh records. Error bars of organic geochemical data represent standard deviations of 2-3 analyses

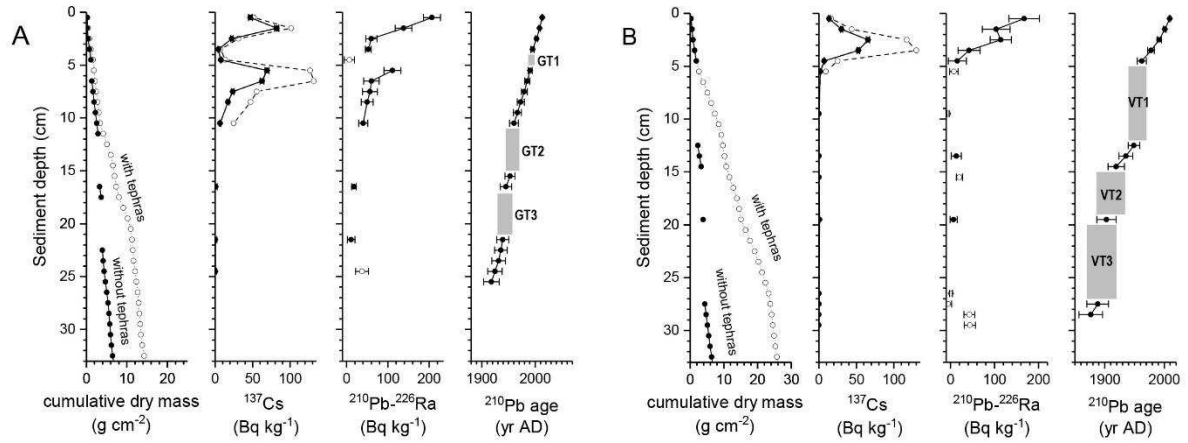

746

747 **Fig. 3** Cumulative dry mass, activities of ^{137}Cs (solid symbols: original data, open symbols: decay-
748 corrected data), excess ^{210}Pb, and ^{210}Pb ages of the upper 35 cm of GEM17-1 (A) and VER17-1 (B).
749 Dates given represent mean ^{210}Pb ages, bars represent maximum and minimum possible ages. Excess
750 ^{210}Pb values used for the age models are given with solid symbols. The maximum and minimum age
751 ranges of tephra layers are shown as grey bars

752

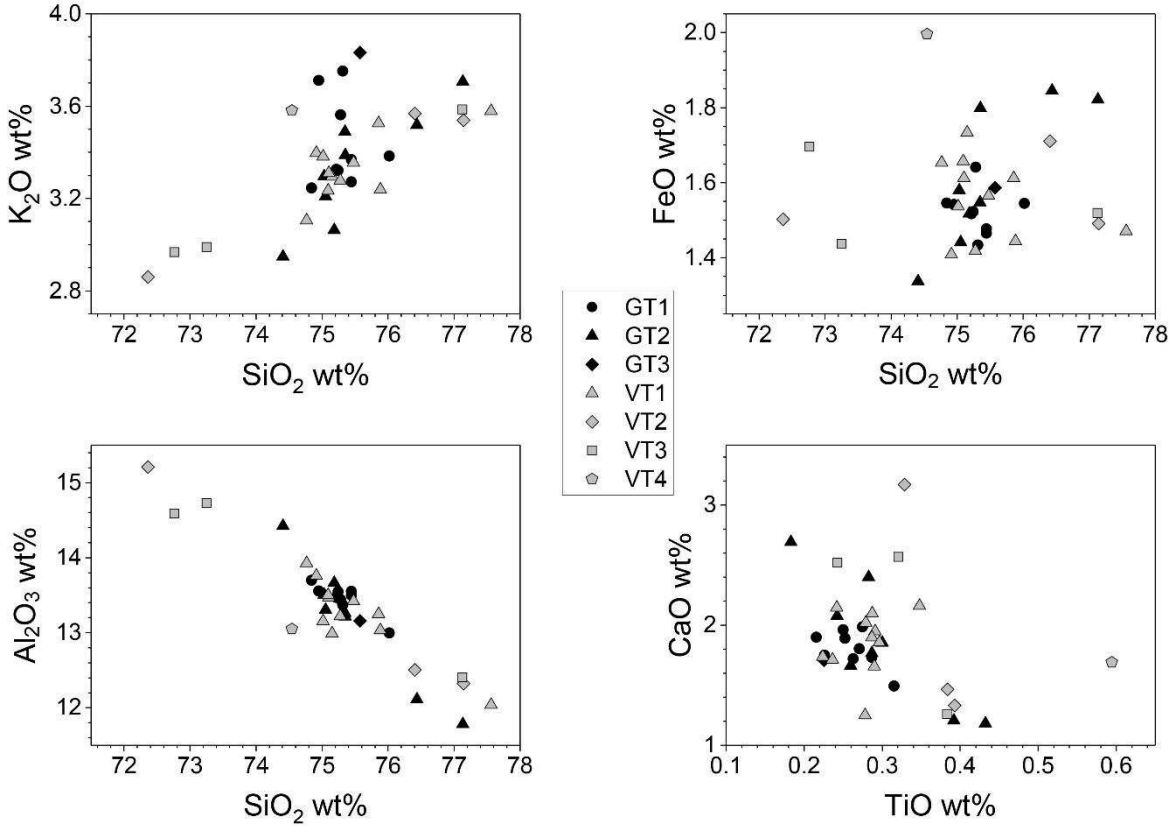

753

754 **Fig. 4** Variation diagrams of glass-chemical data identified from tephra layers in GEM17-1 (GT1-3) and
755 VER17-1 (VT1-4) sediment cores. Each data point represents one analysed glass shard. For average
756 chemical composition of tephras, see Table 1

757

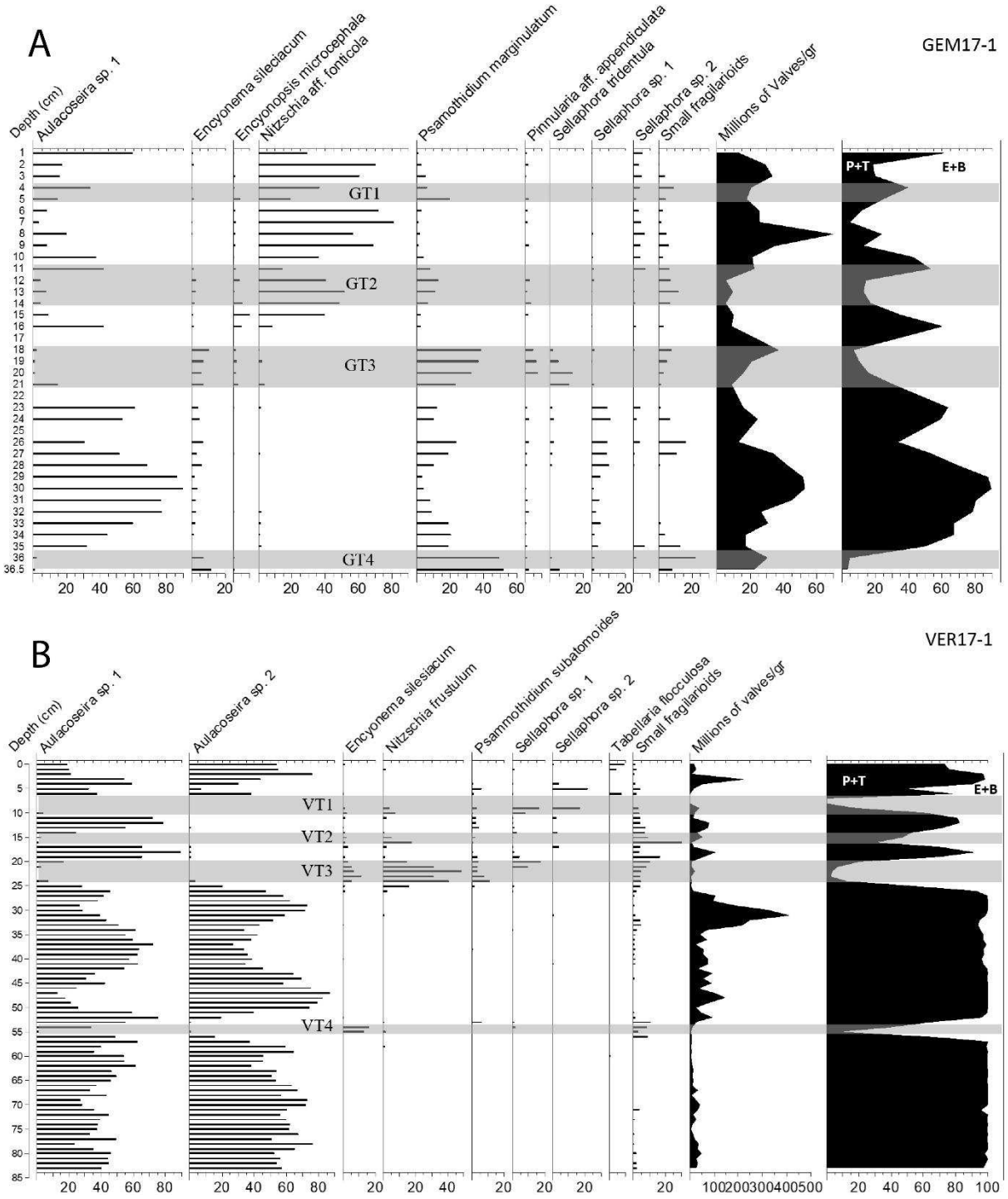

Fig. 5 Assemblages of the most important diatom taxa (in percent), total diatom concentration (log scale) and percentage of benthic and epiphytic (B+E) versus planktonic and tychoplanktonic (P+T) diatom taxa in cores GEM17-1 (A) and VER17-1 (B). Only taxa that occurred with an abundance >5% in at least 2 samples are shown

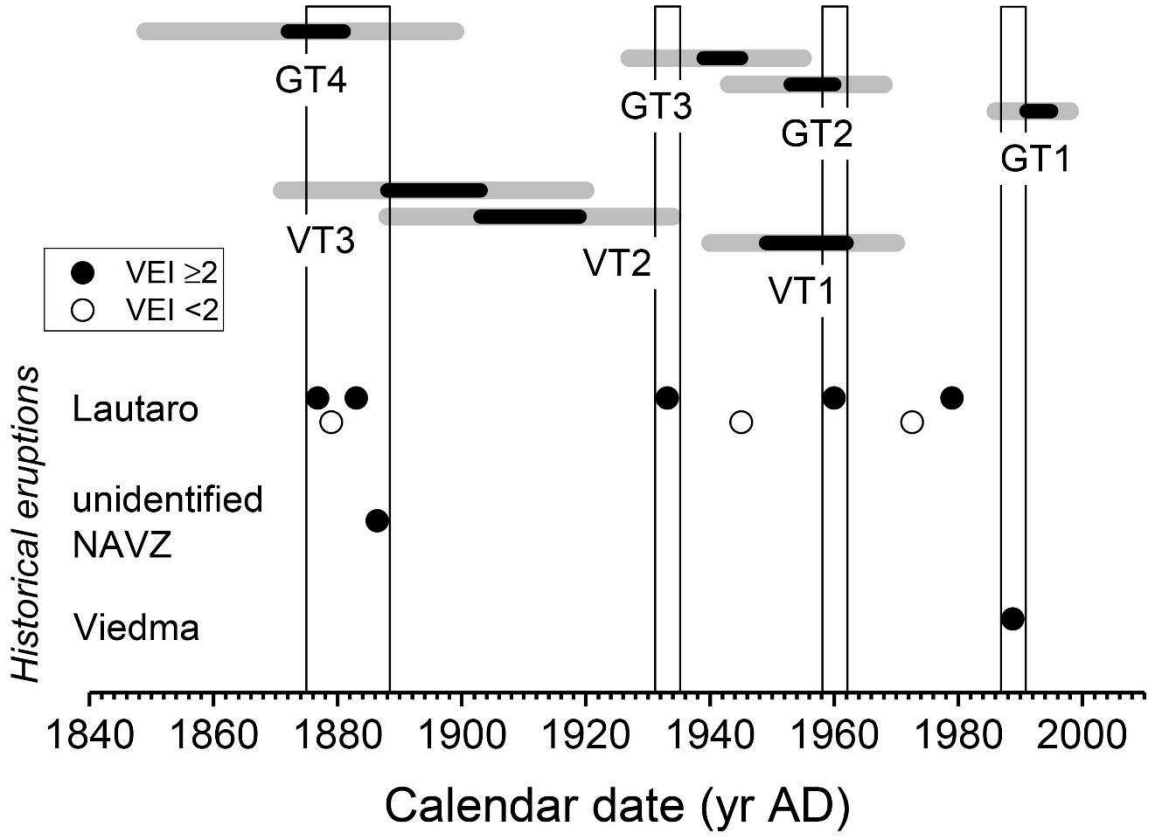

765

766 **Fig. 6** Schematic timeline of historical eruptive events of Lautaro, Viedma, and an eruption of an
767 unidentified NAVZ volcano as recorded in the literature (Table 2), against tephra layers identified in
768 Lagunas Verde (VT1-3) and Gemelas Este (GT1-4), which were chronologically constrained using ^{210}Pb
769 measurements. Filled circles represent high-explosivity events and open circles low-explosivity events.
770 Ages are presented using the lower and upper age estimates by black bars, and maximum and minimum
771 errors as grey lines. Vertical bars highlight the historical volcanic eruptions most likely present in the
772 lacustrine tephra records with a volcanic explosivity index (VEI) ≥ 2

773

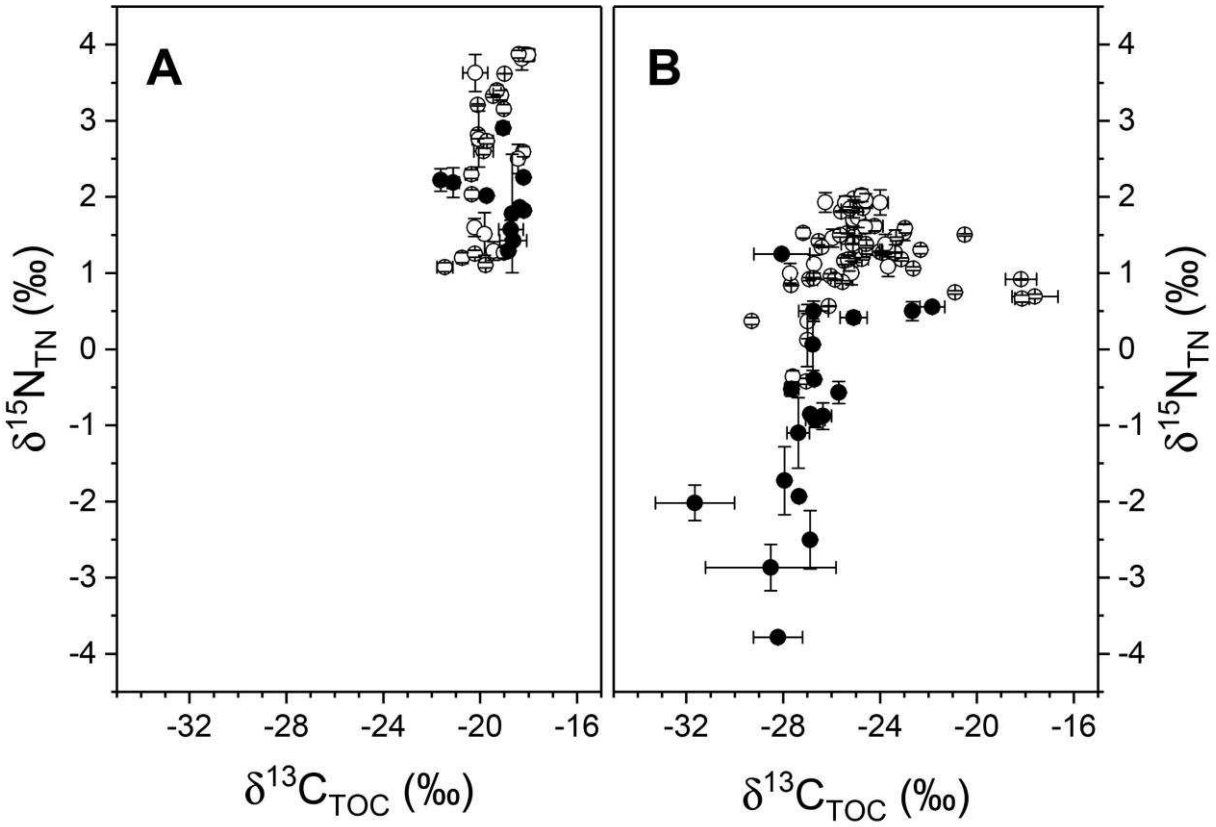

Fig. 7 $\delta^{15}N_{TN}$ versus $\delta^{13}C_{TOC}$ values for GEM17-1 (A) and VER17-1 (B). Sediment layers containing tephra (black circles) are optically distinguished from those without tephra (open circles). In VER17-1 $\delta^{15}N_{TN}$ values in the tephras are lower than in the rest of the sediment which is not the case for GEM17-1

780 **Table 1** Individual glass-shard major elemental composition (means and standard deviations) from
781 seven tephras identified in GEM17-1 (GT1-3) and VER17-1 (VT1-4)

Label		SiO_2	TiO_2	Al_2O_3	FeO	MnO	MgO	CaO	Na_2O	K_2O	P_2O	Cl	Total
GT1	*avg*	75.31	0.26	13.46	1.52	0.03	0.29	1.80	3.66	3.44	0.04	0.19	96.86
n=9	sdev	0.34	0.03	0.20	0.06	0.03	0.04	0.15	0.16	0.19	0.02	0.03	1.96
GT2	*avg*	75.49	0.30	13.16	1.61	0.03	0.28	1.86	3.70	3.33	0.07	0.18	97.48
n=8	sdev	0.87	0.08	0.85	0.19	0.04	0.06	0.53	0.15	0.25	0.04	0.02	1.52
GT3	*avg*	75.57	0.23	13.16	1.59	0.05	0.20	1.71	3.51	3.83	0.07	0.09	98.11
n=1													
VT1	*avg*	75.46	0.28	13.25	1.56	0.04	0.26	1.86	3.73	3.34	0.05	0.18	97.46
n=11	sdev	0.78	0.03	0.49	0.11	0.04	0.07	0.27	0.28	0.13	0.03	0.03	1.61
VT2	*avg*	75.30	0.37	13.35	1.57	0.03	0.19	1.99	3.68	3.32	0.05	0.15	96.94
n=3	sdev	2.57	0.03	1.62	0.12	0.03	0.05	1.03	0.44	0.40	0.05	0.02	1.15
VT3	*avg*	74.38	0.32	13.91	1.55	0.04	0.28	2.12	3.96	3.18	0.12	0.15	97.54
n=3	sdev	2.39	0.07	1.30	0.13	0.03	0.17	0.74	0.72	0.35	0.09	0.04	2.51
VT4	*avg*	74.55	0.59	13.05	2.00	0.00	0.40	1.69	3.92	3.58	0.16	0.06	98.92
n=1													

782

783 **Table 2** Historic eruptions in the NAVZ. VEI was obtained from the Global Volcanism Program
784 (2013), except for the eruptions of 1883 and 1886, which were estimated from historic descriptions, as
785 referenced

786

Volcano	Year of eruption	VEI	Reference
Viedma	1988	2	Kilian (1990)
Lautaro	1978/79	2	Lliboutry (1998)
Lautaro	1972	1	Lliboutry (1998)
Lautaro	1959/60	2	Martinic (1988)
Lautaro	1945	1	Lliboutry (1998)
Lautaro	1933	2	Martinic 1988
Unidentified, NAVZ	1886	≥2	Burmeister (1891)
Lautaro	1883	≥2	Martinic 2016
Lautaro	1878/79	?	Martinic 2008
Lautaro	1876	2	Martinic 1988

787

788